MISSION ANALYSIS AND NAVIGATION ASSESSMENT FOR HERA'S MILANI CUBESAT

C. Bottiglieri [(1)], F. Piccolo [(2)], A. Rizza [(3)], M. Pugliatti [(4)], V. Franzese [(5)], C. Giordano [(6)], F. Ferrari [(7)], F. Topputo [(8)]

[(1)] Department of Aerospace Science and Technology, Politecnico di Milano, Via la Masa 34, 20156 Milano, Italy. +39 02 2399 7158, claudio.bottiglieri@polimi.it
[(2)] Department of Aerospace Science and Technology, Politecnico di Milano, Via la Masa 34, 20156 Milano, Italy. +39 02 2399 7158, felice.piccolo@polimi.it
[(3)] Department of Aerospace Science and Technology, Politecnico di Milano, Via la Masa 34, 20156 Milano, Italy. +39 02 2399 7158, antonio.rizza@polimi.it
[(4)] Department of Aerospace Science and Technology, Politecnico di Milano, Via la Masa 34, 20156 Milano, Italy. +39 02 2399 7158, mattia.pugliatti@polimi.it
[(5)] Department of Aerospace Science and Technology, Politecnico di Milano, Via la Masa 34, 20156 Milano, Italy. +39 02 2399 7158, vittorio.franzese@polimi.it
[(6)] Department of Aerospace Science and Technology, Politecnico di Milano, Via la Masa 34, 20156 Milano, Italy. +39 02 2399 7158, carmine.giordano@polimi.it
[(7)] Department of Aerospace Science and Technology, Politecnico di Milano, Via la Masa 34, 20156 Milano, Italy. +39 02 2399 7158, fabio1.ferrari@polimi.it
[(8)] Department of Aerospace Science and Technology, Politecnico di Milano, Via la Masa 34, 20156 Milano, Italy. +39 02 2399 7158, francesco.topputo@polimi.it

ABSTRACT

Hera is the European contribution to the ESA-NASA collaboration AIDA. During the mission, two CubeSats will be released in proximity of the binary asteroid 65803-Didymos: Milani and Juventas. In this work, an updated overview about the Milani mission analysis and navigation assessment are presented. The mission profile and the trajectories are shown. Then, a navigation assessment is presented, and the results are shown for the main phases of the mission.

1 INTRODUCTION

In 2027, Hera will rendezvous with the binary asteroid 65803 Didymos as the European contribution to AIDA [1] (Asteroid Impact and Deflection Assessment) between ESA and NASA, the latter being responsible for the Double Asteroid Redirection Test (DART) kinetic impactor spacecraft [2]. In proximity of the target, Hera will release two CubeSats Milani and Juventas. The two nanosatellites will be the first CubeSats to perform long term scientific and technological operations around a binary asteroid. Milani is a 6U CubeSat with 6 DOF manoeuvring capabilities to control both translational and attitude motions. The main scientific goals of Milani are to obtain a detailed mapping and characterization of the asteroids' surfaces with the ASPECT [3] hyperspectral imager and to acquire high quality images of the crater produced on the secondary (Dimorphos) by DART. A secondary payload, VISTA [4], will be employed to characterize the dust environment around the asteroids. Milani will communicate with ground via Hera through an Inter-Satellite Link (ISL) making the CubeSat a unique opportunity for technological in orbit demonstration. The project is led by Tyvak International. Politecnico di Milano is responsible for the mission analysis and Guidance, Navigation, and Control (GNC) subsystem design.

Various works in the literature are sprouting illustrating different aspects of the Milani mission. The most relevant ones are briefly listed here for the interested reader to provide context for what is presented and what is omitted in this work. The process of designing close-proximity operations in a binary asteroid system is discussed at length in [5] while the preliminary mission analysis and GNC design of Milani, which constituted the proposal and phase 0 of the mission, are illustrated in [6]. A partial description of the on-board Image Processing (IP) of Milani can be found in [7], which also contains a performance assessment of one of the algorithms presented in this work against machine learning methods. A complete description of the IP is instead discussed at length in [8]. This same algorithm is tested in a Hardware-In-The-Loop facility in [9], illustrating its robustness to varying conditions. A detailed overview of the mission and its semi-autonomous vision-based GNC system is illustrated in [10], while in [11] the important relationship between the trajectory design and orbit determination processes is shown.
This work is focused on an updated overview about the Milani mission analysis and navigation assessment. After a brief introduction on the asteroid, the reference frame used and the dynamical environment, the mission profile is presented, and the navigation assessment on Milani main phases is shown.

1.1 Didymos properties

Didymos is a binary Near-Earth Asteroid (NEA) of S-type discovered in 1996 formed by Didymos, or D1 (the primary) and Dimorphos, or D2 (the secondary). Up-to-date data about Didymos and Dimorphos are reported in Table 1.

Table 1: (Top) Binary system parameters (semi-major axis, eccentricity, inclination, revolution period. (Bottom) Didymos and Dimorphos mass and spin periods properties as in [12].

System Parameters			
a	**e**	**i**	**T**
1.66446 AU	0.3839	3.4083°	770 days
Asteroids Parameters			
M_1	**M_2**	**T_1**	**T_2**
5.226×10^{11} kg	4.860×10^{9} kg	2.26 h	11.92 h

The orbital properties are retrieved from the up-to-date kernels of the Hera mission. In the up-to date reference model, Dimorphos and Didymos are assumed to share the same equatorial plane on which their relative motion occurs and Dimorphos is assumed to be in a tidally locked configuration with Didymos. In this work, two reference frames are used. “DidymosEclipJ2000” is a quasi-inertial reference frame, centred in the system barycentre with the axis directed as the inertial EclipJ2000 reference frame. This frame can be considered inertial for intervals of time negligible with respect to Didymos heliocentric motion. “DidymosEquatorialSunSouth” is a non-inertial reference frame in which the trajectories are shown. It is centred in the system barycentre and has the xy plane on the asteroid equatorial plane. The x-axis is aligned with the projection of the Sun vector on the equatorial plane and the z-axis is aligned to the south pole of Didymos.

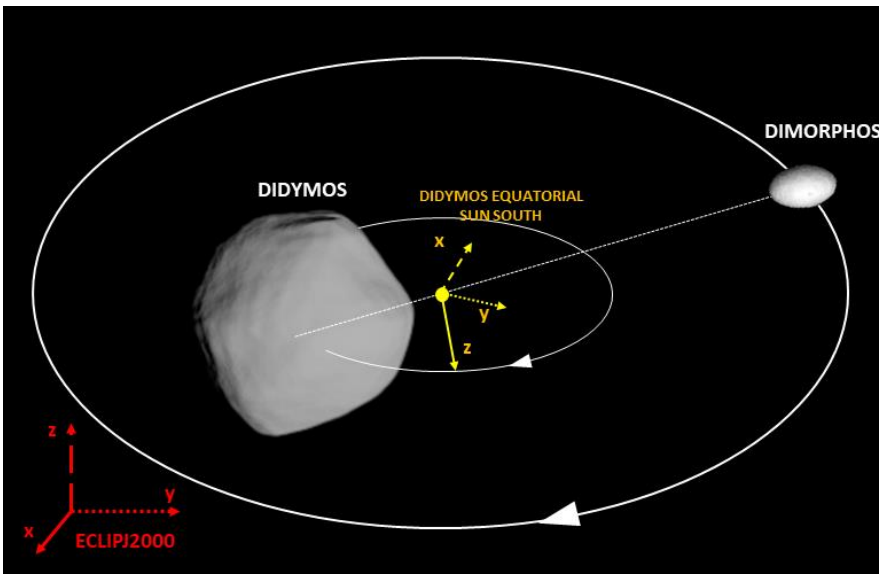

Figure 1: Didymos geometry. The reference frames are highlighted. The red frame is the inertial Eclip2000 which corresponds to the quasi-inertial DidymosEclipJ2000 when centred in the system barycentre. The yellow frame is the DidymosEquatorialSunSouth

2 DYNAMICAL ENVIRONMENT

The dynamics around Didymos are modelled according to the perturbed Restricted Three-Body Problem (R3BP). Although shape-based models are available for the asteroids' gravity, point like masses are considered for the purpose of this work. Indeed, the minimum distance reached by Milani during its scientific observations is higher than 800 m, the altitude at which the irregularities of the gravity field become important [5]. The main perturbation is the Sun as a fourth body and in the form of Solar Radiation Pressure (SRP) which far from the system (>10 km) can be dominant with respect to the asteroids' gravity. The equation of motion for Milani in the DidymosEclipJ2000 reference frame can be written as

$$\ddot{\boldsymbol{r}} = -\mu_1 \frac{\boldsymbol{r}_1}{r_1^3} - \mu_2 \frac{\boldsymbol{r}_2}{r_2^3} + \boldsymbol{a}_{4body} + \boldsymbol{a}_{SRP} \tag{1}$$

Where $\mathbf{r}$ is the CubeSat position with respect to the system barycentre, μ_1 and μ_2 are the standard gravitational parameters of the primary and the secondary asteroid, while $\mathbf{r}_1$ and $\mathbf{r}_2$ are the CubeSat relative position with respect to them. $\mathbf{a}_{4body}$ is the gravity perturbation of the Sun and it has been simply modelled as

$$\boldsymbol{a}_{4body} = -\mu_S \left(\frac{\boldsymbol{r}_S}{r_S^3} - \frac{\boldsymbol{r}_{DS}}{r_{DS}^3} \right) \tag{2}$$

Where μ_S is the Sun gravity constant, $\mathbf{r}_S$ is the relative position of the third body with respect to the Sun and $\mathbf{r}_{DS}$ is the position of the system with respect to the Sun. Instead, the SRP has been modelled with a cannonball model

$$\boldsymbol{a}_{SRP} = \frac{P_0}{c} \left(\frac{r_{SE}}{r_S} \right)^2 \frac{C_r A}{m} \frac{\boldsymbol{r}_S}{r_S} \tag{3}$$

Where, P0 (1367 W/m^2) is the solar flux at 1 AU, c is the speed of light, r_{SE} is the Sun-Earth distance (1 AU), Cr is the reflectivity coefficient of the CubeSat, A is its equivalent surface area, and m is the CubeSat mass.

3 MISSION PROFILE

Milani trajectory design has been mainly driven by the main scientific goals of the mission, but it has also been influenced by both technical and operational constraints. Due to the low gravity environment around the asteroids, selecting Keplerian orbits as nominal trajectories would require a demanding station keeping strategy to cope with the SRP effect. For this reason, a patched-arc manoeuvring strategy that leverage the SRP acceleration to target pre-selected waypoints has been implemented. This strategy has flight heritage in small-body environment. It is the one currently envisaged by the Hera spacecraft during its operational phases and previously performed by the Rosetta spacecraft during its initial scientific phase, after rendezvous with comet 67-P/Churyumov-Gerasimenko. The waypoints selection has been mostly influenced by the passive nature of Milani's payload that forces the CubeSat to avoid the night-side. The resulting trajectories are loop orbits with manoeuvres points placed as far away from each other as possible to maximize the time spent in proximity to the system [6].
Two phases have been designed to achieve all the scientific goals of the mission: a Far Range Phase (FRP) and a Close Range Phase (CRP).

3.1 Scientific goals and operational constraints

Milani scientific phases design has been mostly driven by its main payload, ASPECT. ASPECT is a passive payload, equipped with a visible to near-infrared hyperspectral imager and will be used on Milani to perform global mapping of the asteroids with detailed observation of the DART crater on Dimorphos. ASPECT main scientific goals can be summarized in three actions:

1. Imaging both the asteroids with a spatial resolution better than 2 m/pixel
2. Imaging the secondary asteroid with a spatial resolution better than 1 m/pixel
3. Imaging the DART crater with a spatial resolution better than 0.5 m/pixel at phase angle (Sun-asteroid-Milani angle) in the range [0-10] deg and [30-60] deg.

In terms of trajectory design, spatial resolution requirements drive the maximum range at which scientific observations can be performed. Operationally, Milani is constrained to communicate with ground via an Inter-Satellite Link (ISL) using Hera as data relay. Consequently, Milani shall adopt the same uplink and downlink window of the main spacecraft. Thus, Milani's manoeuvring schedule shall be aligned with Hera's to avoid open loop manoeuvring. Once the information is loaded, Milani can accumulate delay with Hera by manoeuvring later in time. However, as the time between the downlink of the observables and the manoeuvre execution increases, the accuracy of the correction manoeuvre decreases. The minimum time assumed for Milani between these two events is of 49 h, which is 1 h plus the assumed Turn-Around Time (TAT), the time between the download of navigation information and the upload of the instructions.

3.2 Far Range Phase – FRP

The complete mapping of the bodies with a resolution better than 2 m/pixel with ASPECT can be achieved with observations at a distance lower than 11 km from the surface. This is accomplished during the Far Range Phase in which Milani hoovers over the bodies in a repetition of loop orbits quasi-symmetric with respect to the Sun direction. Figure 2 shows the trajectory as a 6-points hyperbolic loop with a manoeuvring pattern of 4-3 days repeated three times.

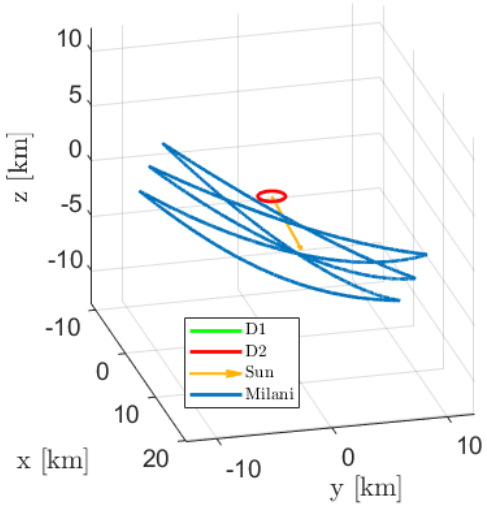

Figure 2: FRP trajectory in DidymosEquatorialSunSouth

3.3 Close Range Phase – CRP

The complete mapping of the bodies with a resolution better than 1 m/pixel and the DART crater observations are achieved during Close Range Phase. Being the latter the most challenging goal of the phase, with a maximum distance requirement of 2.78 km from D2, the CRP design has been focused on the crater observation. Instead, the complete mapping is a by-product of this phase. Due to the tidally locked nature of the system, the observation of a feature fully illuminated and visible is constrained to be performed only in specific configurations of the two bodies. In this case, since the DART crater will be on the leading side of D2, the crater can be visible and illuminated only around the D2 dawn at each revolution of D2 around D1. Fulfilling both the resolution and phase angle constraints, when D2 is in that configuration, while respecting the operational constraints on the manoeuvring frequency and the permanence into the dayside, makes impossible to adopt the same trajectory design strategy adopted for the FRP. Consequently, a slightly modified waypoints strategy has been used for the CRP design. Indeed, CRP design is based on the selection of KeyPoints [11]. A KeyPoint is the position at which the satellite can perform the desired scientific observation fulfilling all the requirements. Thus, while the relative position of the KeyPoints ensures the fulfilling of the scientific requirements, the manoeuvring points position serves to comply with the constraints and to ensure the flyability of the trajectory. Indeed, CRP design has been performed in an iterative fashion considering the navigation assessments results to make it robust to uncertainty and increase its flyability. In fact, many CRP arcs last 7 days, to allow for a correction manoeuvre execution in the middle of a nominal ballistic arc. Furthermore, at the end of CRP, Milani will be injected into a Sun Synchronous Terminator Orbit (SSTO) and to facilitate this plane change, during CRP, Milani slightly increases its declination with respect to the equatorial plane.

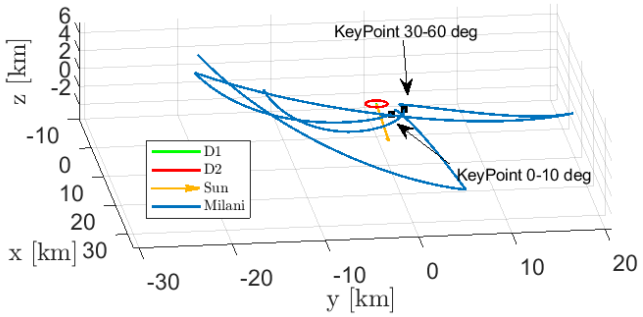

Figure 3: CRP trajectory in DidymosEquatorialSunSouth

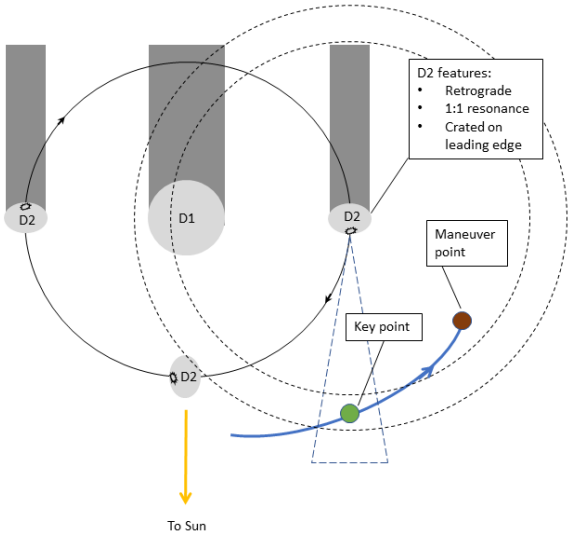

Figure 4: The choice of the "Key Point" where the CubeSat can image the crater on Dimorphos at optimal illumination conditions, at required distance and phase angle. The manoeuvre points of the observation arcs are chosen to avoid going into the night-side

4 NAVIGATION ASSESSMENT

Once the nominal mission profile is designed, a navigation assessment is necessary to understand the off-nominal performances in terms of state estimation and distance between the real trajectory flown and the nominal one. This analysis can be seen as an assessment of the flyability of a nominal trajectory and it is performed through two analyses: a knowledge analysis and a dispersion analysis.

4.1 Knowledge Analysis

The knowledge analysis (KA) assesses the achievable level of accuracy in the spacecraft state knowledge. Indeed, the knowledge is the difference between the estimated trajectory and the real one. The analysis starts with an initial knowledge modelled as a gaussian distribution, centred in the nominal state with a given initial covariance, which is propagated forward. During the propagation the covariance increases due to the uncertainties affecting the dynamics and decrease during an orbit determination (OD) process. During an OD, an Extended Kalman Filter (EKF) is used to process the measurements taken and give an estimation of the spacecraft state. Random errors and biases are considered as in Schimdt's formulation [13]. Propagation is made linearly using the nominal state transition matrix (STM), as done in [14].

Milani's navigation is optical based with the support of radiometric information about range and range-rate of the CubeSat with respect to Hera. Image processing is implemented both on-board with centroiding algorithms with the aim of supporting autonomous pointing and on-ground with landmark-based methods supporting the navigation. The optical measurement employed in the EKF is a single position vector of the spacecraft from the centre of D1, affected by an equivalent error function of the nominal range representing the error sources of a landmark-based method shown in Equation 4 for the range and Equation 5 for the transversal angle error. Landmark-based methods are assumed to be feasible at distances lower than 14 km from the asteroid. For higher distances, a centroiding approach has been implemented. The remaining uncertainties considered in the analysis are summarized in Table 2. SRP and residual acceleration are treated as Gauss-Markov process as in [14] with a correlation time of 1 day.

$$f_r = c_{r0} + c_{r1} r \tag{4}$$

$$f_\theta = arctan\left(\frac{c_{\theta 0}}{r}\right) + c_{\theta 1}\sqrt{r} \tag{5}$$

where c_{r0} = 0.44, c_{r1} = 2.5 x 10^{-5} m^{-1}, $c_{\theta 0}$ = 2.35 m and $c_{\theta 1}$ = 1.4251 x 10^{-6} $m^{-1/2}$

Table 2: Uncertainties affecting Milani's navigation and dynamic environment

Source of uncertainty	Modelled as	Value [1-sigma]
Thruster	Noise	1.67% magnitude, 0.67 deg direction
SRP	Gauss Markov	8% magnitude
Residual acceleration	Gauss Markov	5 x 10^{-9} m/s^2
Gravity uncertainty	Estimation Parameter	10^{-4} m^3/s^2
ISL – Range	Noise (Bias)	0.5 m (150 m)
ISL – Range rate	Noise (Bias)	1.5 cm/s (3 cm/s)

The flight dynamic (FD) team exploits the knowledge to evaluate the correction manoeuvres during the mission using the estimated state deviation. However, since 48 h are assumed to be needed for the FD operations from the downlink of the observables and the uplink of the information, the measurements taken after the downlink of the observables cannot be used for the operations of the current arc, but they will be useful for the next cycle of operations. Thus, the results section will show graphs with an additional knowledge (dashed black line) represented by the covariance used by the FD for the correction manoeuvre estimation, which is the covariance sent to ground at downlink simply propagated forward.

4.2 Dispersion Analysis

The dispersion analysis (DA) shows the statistics of the nominal trajectory from the real one. Indeed, the dispersion is the stochastic distance between the real trajectory and the nominal one. DA can be performed with a Monte Carlo analysis. For each iteration, the deviated parameters as the initial state, the gravitational parameters or the thruster accuracy, are selected from a gaussian distribution centred in the nominal parameters with a given covariance. The analysis is performed through a forward propagation of the deviated state using the deviated dynamics. During the propagation dispersion increases and can decrease after the execution of correction manoeuvres. Correction manoeuvres are computed from the estimated deviation from the nominal state at manoeuvre obtained as the propagation of the perturbed deviated state from the downlink to the manoeuvre point. The perturbation is given by the knowledge covariance at downlink. Usually, for deep-space operations a correction manoeuvre is scheduled each week, but for Milani a correction manoeuvre is foreseen at the earliest convenience, each 3 and 4 days, in compliance with the operational constraints. Differential guidance [15] is the guidance strategy adopted for Milani. Largely used for interplanetary missions, the whole trajectory is subdivided in different legs with this algorithm. At the extremal points of a leg, two manoeuvres are applied to cancel both the position and the velocity deviation on the final leg point. The final impulse is usually not applied in practice, since at the time of arrival at that point, a new manoeuvre is calculated. Thus, the correction manoeuvre is computed by minimizing the deviation from the nominal state at the final point in a least square residual sense. The resulting manoeuvre to be applied at time t_j to cancel deviations at time t_{j+1} is computed as

$$\boldsymbol{\Delta v}_j = -(\boldsymbol{\Phi}_{rv}^T \boldsymbol{\Phi}_{rv} + q\boldsymbol{\Phi}_{vv}^T \boldsymbol{\Phi}_{vv})^{-1}(\boldsymbol{\Phi}_{rv}^T \boldsymbol{\Phi}_{rr} + q\boldsymbol{\Phi}_{vv}^T \boldsymbol{\Phi}_{vr})\widetilde{\delta \boldsymbol{r}_j} - \widetilde{\delta \boldsymbol{v}_j} \quad (6)$$

Where δr_j and δv_j are the estimated position and velocity deviation, $\boldsymbol{\Phi}_{rr}$, $\boldsymbol{\Phi}_{rv}$, $\boldsymbol{\Phi}_{vr}$, $\boldsymbol{\Phi}_{vv}$ are the 3-by-3 blocks of the STM $\boldsymbol{\Phi}$ from time t_j to time t_{j+1} associated to the nominal trajectory, and q adjusts the dimensions. The uncertainties affecting the dynamic considered are the one described in Table 2.

4.3 Results

Results for FRP and CRP are presented in ECLIPJ2000 frame. Figure 5, Figure 6, Figure 7 and Figure 8 show the position and velocity standard deviations predicted by the filter during FRP and CRP. In particular, the square roots of the diagonal elements of the covariance matrix are shown. The total knowledge, represented in black, is obtained as the root sum squared of the diagonal elements. The

dashed black line is the total knowledge available on ground for the OD process. Manoeuvres, optical navigation images and cut-off times (downlink instants) are shown with dashed vertical lines, while ISL measurement windows are highlighted in grey. Different measurements campaigns are adopted for the two phases due to the different nature of the two trajectories. During CRP, the optical navigation performances are lower around the 10th and 35th day since Milani is getting further from the system and landmark-based methods cannot be applied.

Figure 9, Figure 10, Figure 11 and Figure 12 show the dispersion analysis results in terms of dispersion and navigation costs. The dispersion is shown in its absolute value as the distance with respect to the nominal trajectory (black) and in a relative form as the ratio between the absolute dispersion and nominal range with respect to the bodies (red). FRP appears to be robust with respect to uncertainties while the demanding scientific requirements of CRP and the high uncertainty on the thruster make the CRP riskier. In particular, the relative dispersion is close to the higher boundary of 33% 1-sigma, for which a not-negligible collision risk is present.

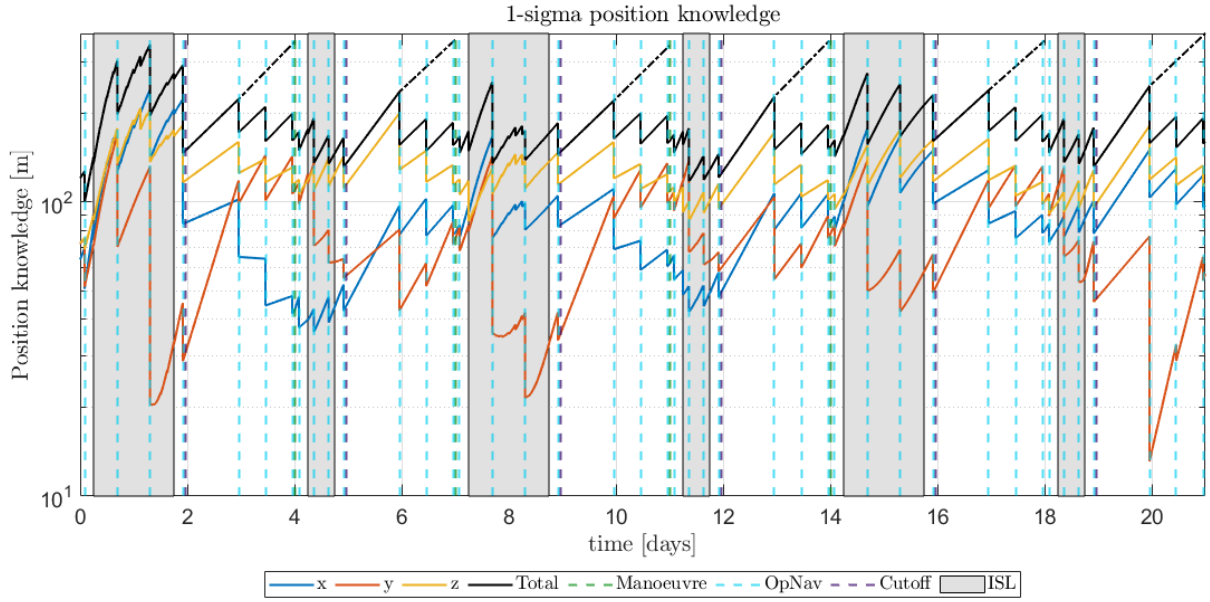

Figure 5: 1-sigma position knowledge during the FRP. The dashed black line is the knowledge obtained considering only observables generated before downlink.

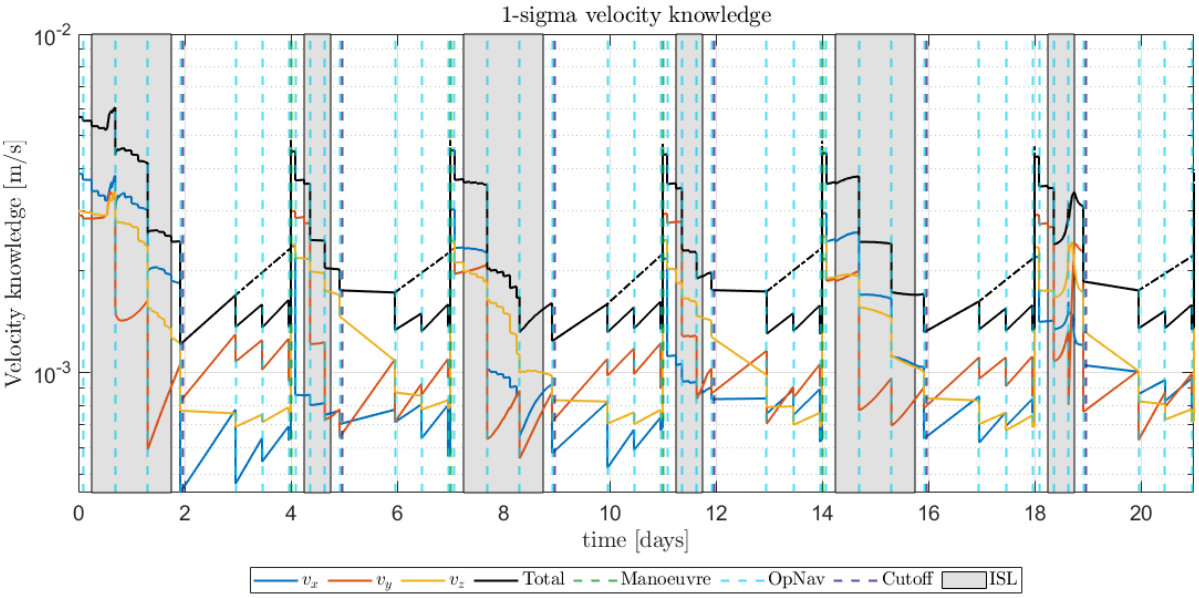

Figure 6: 1-sigma velocity knowledge during the FRP. The dashed black line is the knowledge obtained considering only observables generated before downlink.

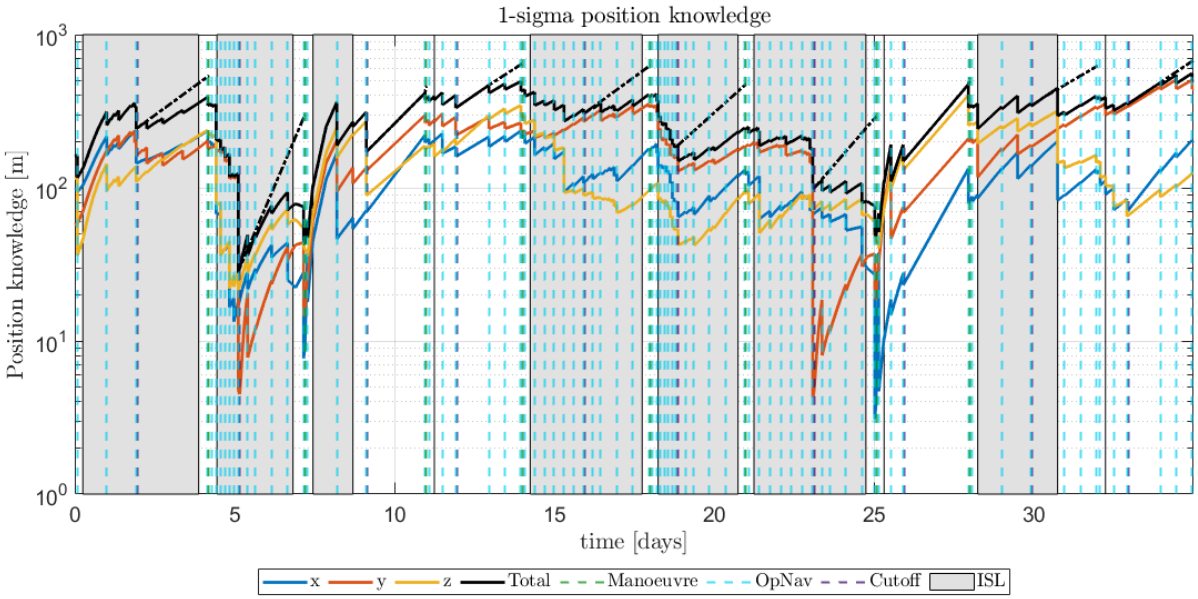

Figure 7: 1-sigma position knowledge during the CRP. The dashed black line is the knowledge obtained considering only observables generated before downlink.

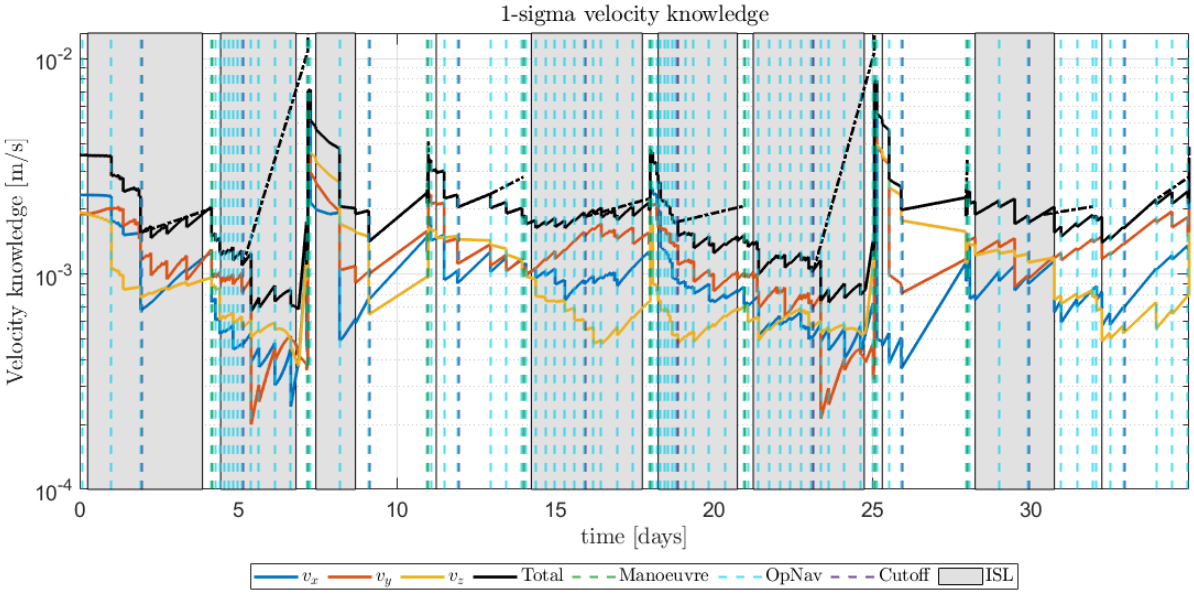

Figure 8: 1-sigma velocity knowledge during the CRP. The dashed black line is the knowledge obtained considering only observables generated before downlink.

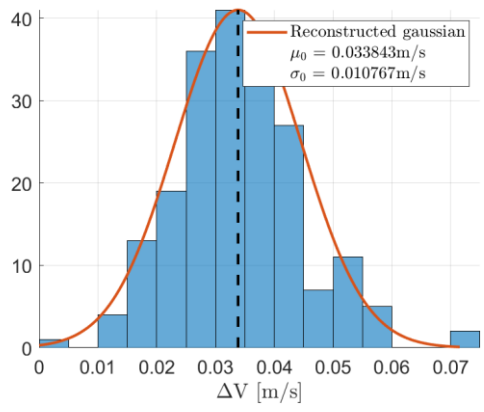

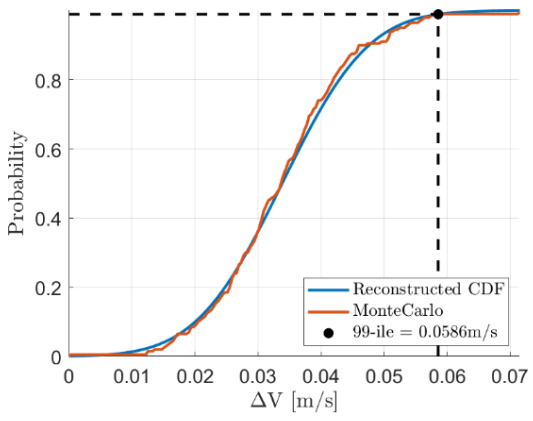

Figure 9: Navigation cost for FRP. On the left probability distribution function. On the right cumulative distribution function.

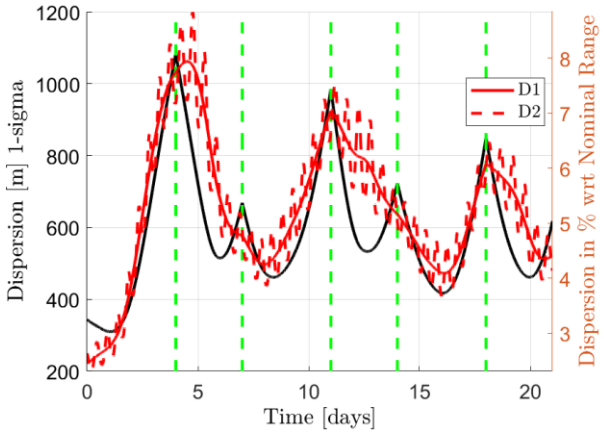

Figure 10: 1-sigma dispersion during the FRP, absolute value on the left (black), % value with respect to nominal range on the right (red). Dashed green lines are the manoeuvres instants.

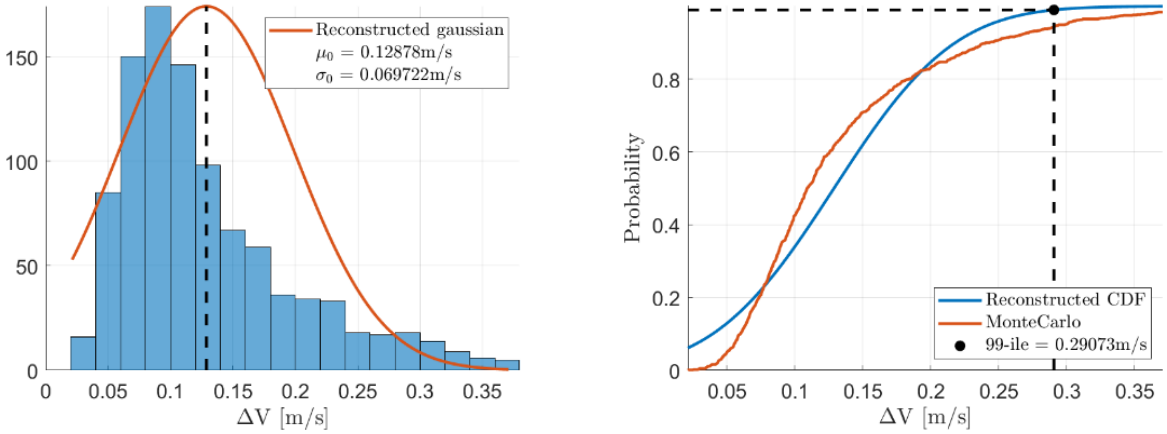

Figure 11: Navigation cost for CRP. On the left probability distribution function. On the right cumulative distribution function.

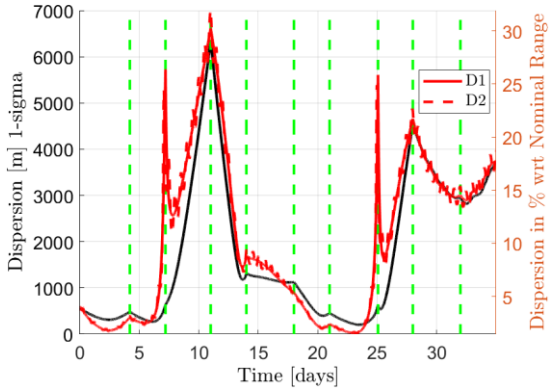

Figure 12: 1-sigma dispersion during the CRP, absolute value on the left (black), % value with respect to nominal range on the right (red). Dashed green lines are the manoeuvres instants.

5 CONCLUSIONS

This paper is focused on Milani trajectory design and navigation assessment. The complexity of orbiting in a highly perturbed low-gravity environment is increased using miniaturized components and considering the relative operational constraints. The solutions presented clearly show how the design gets more complex when the CubeSat needs to get closer to the system. During the Close Range Phase the spacecraft must get very close to Dimorphos. Thus, it requires a complex asymmetric design with the definition of KeyPoints at which Milani can perform science and a concurrent phasing with the motion of Dimorphos and the manoeuvring schedule of Hera. Instead, the non-scientific arcs are designed to reduce the accumulated dispersion after the expensive manoeuvre performed close to the system when Milani moves fast. The thruster error is proportional to the manoeuvre magnitude and Milani needs to get farther from the system to recover its nominal state. Milani navigation and guidance also get more complex during CRP. The measurements campaign is irregular to maximize the filter performances and exploits the optical navigation more often when Milani is closer to the system. Instead, correction manoeuvres are carefully tuned to particularly reduced relative dispersion to avoid collision risks.

6 ACKNOWLEDGMENT

This work has been performed under Tyvak International contract within the scope of ESA Contract No. 1222343567/62/NL/GLC. The authors would like to acknowledge the support received by the whole Milani Consortium. M.P and F.T would like to acknowledge the funding received from the European Union's Horizon 2020 research and innovation programme under the Marie Skłodowska-Curie grant agreement No 813644.

7 REFERENCES

[1] Cheng, A., Atchison, J., Kantsiper, B., Rivkin, A., Stickle, A., Reed, C., Galvez, A., Carnelli, I., Michel, P., and Ulamec, S., "*Asteroid Impact and Deflection Assessment mission*," Acta Astronautica, Vol. 115, 2015, pp. 262–269. https://doi.org/10.1016/j.actaastro.2015.05.021.

[2] Sarli, B. V., Atchison, J. A., Ozimek, M. T., Englander, J. A., and Barbee, B. W., "*Double Asteroid Redirection Test Mission: Heliocentric Phase Trajectory Analysis*," Journal of Spacecraft and Rockets, Vol. 56, No. 2, 2019, pp. 546–558. https://doi.org/10.2514/1.A34108.19

[3] Kohout, T., Näsilä, A., Tikka, T., Granvik, M., Kestilä, A., Penttilä, A., Kuhno, J., Muinonen, K., Viherkanto, K., and Kallio, E., "*Feasibility of asteroid exploration using CubeSats—ASPECT case study*," Advances in Space Research, Vol. 62, No. 8, 2018, pp. 2239–2244. https://doi.org/10.1016/j.asr.2017.07.036

[4] Palomba, E., Longobardo, A., Dirri, F., Zampetti, E., Biondi, D., Saggin, B., Bearzotti, A., and Macagnano, A., "*VISTA: A μ-Thermogravimeter for Investigation of Volatile Compounds in Planetary Environments*," Origins of Life and Evolution of Biospheres, Vol. 46, No. 2, 2016, pp. 273–281. https://doi.org/10.1007/s11084-015-9473-y.

[5] Ferrari, F., Franzese, V., Pugliatti, M., Giordano, C., and Topputo, F., "*Trajectory Options for Hera's Milani CubeSat Around (65803) Didymos*," The Journal of the Astronautical Sciences, Vol. 68, No. 4, 2021, pp. 973–994. https://doi.org/10.1007/s40295-021-00282-z.

[6] Ferrari, F., Franzese, V., Pugliatti, M., Giordano, C., and Topputo, F., "*Preliminary mission profile of Hera's Milani CubeSat*," Advances in Space Research, Vol. 67, No. 6, 2021, pp. 2010–2029. https://doi.org/10.1016/j.asr.2020.12.034.

[7] Pugliatti, M., Franzese, V. and Topputo, F., *"Data-Driven Image Processing for Onboard Optical Navigation Around a Binary Asteroid",* Journal of Spacecraft and Rockets, Jan. 2022, pp. 1–17. Article in Advance, https://doi.org/10.2514/1.A35213.

[8] Piccolo, F., Pugliatti, M., Panicucci, P., and Topputo, F., *"Toward verification and validation of the Milani Image Processing pipeline in the hardware-in-the-loop testbench TinyV3RSE"*, AAS/GNC 2022, 4-9 Feb 2022.

[9] Pugliatti, M., Franzese, V., Rizza, A., Piccolo, F., Bottiglieri, C., Giordano, C., Ferrari, F., and Topputo, F., "*Design of the on-board image processing of the Milani mission*", AAS/GNC 2022, 4-9 Feb 2022.

[10] Pugliatti, M., Rizza, A., Piccolo, F., Franzese, V., Bottiglieri, C., Giordano, C., Ferrari, F., and Topputo, F., "*The Milani mission: overview and architecture of the optical-based GNC system*," Scitech 2022, 2-7 Jan 2022. https://doi.org/10.2514/6.2022-2381.

[11] Bottiglieri, C., Piccolo, F., Rizza, A., Giordano, C., Pugliatti, M., Franzese, V., Ferrari, F., and Topputo, F., "*Trajectory design and orbit determination for Hera's Milani CubeSat*," AAS/AIAA Astrodynamics Specialist Conference, AAS 21–667, Big Sky, CA, 2021.

[12] Naidu, S., Benner, L., Brozovic, M., Nolan, M., Ostro, S., Margot, J., Giorgini, J., Hirabayashi, T., Scheeres, D., Pravec, P., Scheirich, P., Magri, C., and Jao, J., "*Radar observations and a physical model of binary near-Earth asteroid 65803 Didymos, target of the DART mission*," Icarus, Vol. 348, 2020, p. 113777. https://doi.org/10.1016/j.icarus.2020.113777

[13] Simon, D., *Optimal State Estimation: Kalman, H Infinity, And Nonlinear Approaches*, Wiley, 2006, pp. 309–312.

[14] Tapley, B. D., Schutz, B. E., and Born, G. H., *Statistical Orbit Determination*, Elsevier, 2004, Chap. 4.

[15] Dei Tos, D. A., Rasotto, M., Renk, F., and Topputo, F., "*LISA Pathfinder mission extension: A feasibility analysis*," Advances in Space Research, Vol. 63, No. 12, 2019, pp. 3863–3883. https://doi.org/10.1016/j.asr.2019.02.035.